Palestine Journal of Mathematics

Vol. 11 (Special Issue III)(2022) , 25–40

FINITE ELEMENT ANALYSIS OF OXYGEN TRANSFER FROM BLOOD IN PERMEABLE MICROCIRCULATION TO SURROUNDING TISSUE IN THE PRESENCE OF A MAGNETIC FIELD

Alana R. Sankar, Sreedhara Rao Gunakala and Donna M. G. Comissiong

Communicated by Amit Sharma

MSC 2010 Classifications: Primary 76S05, 76Z05, 92C10 ; Secondary 35Q30, 35Q35, 76-10, 76R50.

Keywords and phrases: Microcirculation, oxygen transfer, permeable vessel walls, magnetic field, two-layered blood flow.

Abstract In order to fully understand what occurs in microcirculation, it is important to examine how oxygen is transferred to tissues and what factors can affect this process. In this numerical study, the transfer of oxygen through permeable vessel walls from microcirculation to tissue was examined in the presence of an external magnetic field. The blood flow was two-layered with a core region as a particle-fluid suspension and a peripheral cell-free plasma layer being considered. In blood, oxygen was assumed to be transported by convection and molecular diffusion while in the tissue region by molecular diffusion and metabolic consumption. A finite element method was utilized in solving the governing equations. The effects of varying hematocrit, core region thickness, magnetic field strength and wall permeability were investigated. It was observed that as hematocrit, C, increased, PO_2 was higher in all three regions. Thus, under conditions where the red blood cell count in the blood is lower than normal, for example in patients with plasma cell dyscrasias or Hb SS-sickle cell, there is less O_2 present which can lead to surrounding tissues becoming starved of O_2. This can result in twitching, dizziness, nausea, seizures and in severe cases can even be fatal. Another factor which increased O_2 is the thickness of the core region. An increase in the core region thickness corresponds to a thinning of the plasma layer. Hence as this peripheral layer thins, the oxygen content elevates in all regions. Increasing the Hartmann number (magnetic field intensity) resulted in a decline in PO_2, thus high intensity magnetic fields should be avoided. Furthermore, some drugs administered can alter vessel wall permeability. There was a decrease in PO_2 as the vessel walls became more permeable with increasing Darcy number. Therefore, the effect that such drugs will have should be closely monitored.

1 Introduction

Oxygen (O_2) transfer plays a vital role in cellular energetics since oxidation and other forms of energy production rely on cells being supplied with oxygen continuously. When air enters the body, through the nose or mouth, it goes to the lungs where oxygen is extracted. This oxygen is then transported by the bloodstream through the circulatory system to tissues where it is used in the mitrochondria of cells. Thus, in order to fully understand the regulation of blood flow, the physical mechanisms of oxygen transport throughout the pathway must be investigated. Oxygen transport within blood, tissue or specific organs is often examined but the study of oxygen transfer from blood vessels to tissue is imperative.

The foundation theory of oxygen transfer to tissue was laid by Krogh [11, page 457]. He proposed that its transport to an elementary tissue unit was by passive diffusion (driven by gradients of oxygen tension) from blood flowing through a single capillary. This model is popularly known as the Krogh's tissue cylinder or Krogh's model. This Krogh's model of oxygen transport between blood capillaries and tissue serves as the foundation for many theoretical studies.

A Finite Element Method (FEM) was used by Kumar [12] to investigate oxygen transport in the capillaries. The Finite Element Method is a useful tool in studying such problems since it

can easily handle problems with an irregular flow geometry and complex boundary conditions. This method was also used to study oxygen transport in the systemic capillaries and surrounding tissues [15, page 107]. Here, the oxygen concentration decreased from the axis of the capillary to the peripheral tissue [15, page 116].

A mathematical model was developed for the simultaneous transport of oxygen and carbon dioxide (CO_2) in the systemic capillaries and surrounding tissue under hyperbaric conditions [16, page 255]. It was found that the concentration of carbon dioxide increased from the axis of the capillary to the peripheral tissue with very little of it being transported radially [16, page 270]. Sharan, Singh and Kumar [17, page 419] proposed a two-layered model to study the effect of the plasma layer on oxygen delivery. An analysis of their results indicated that the plasma layer obstructed oxygen transport from the core region to the tissue [17, page 425].

In the study of oxygen diffusion in the pulmonary capillaries from the alveolar air space to the red blood cells, a finite element model was also utilized [7, page 2036]. A model was created to investigate the effect of hemoglobin-based oxygen carriers (HBOCs) on oxygen transport in capillary sized vessels and the Finite Element Method was used to solve its partial differential equations [21, page 157]. A Finite Element Analysis (FEA) of oxygen transport in microfluidic cell culture devices, with varying channel architectures, perfusion rates and materials, was also performed by Zahorodny-Burke, Nearingburg and Elias [23, page 6244]. A simulation of oxygen transport with moving red blood cells was also done using a dynamic model [13, page 206].

The computational modeling of oxygen transfer in lungs were performed by Kaesler et al. [10, page 786]. Hassanzadeganroudsari et al [9] examined mass transfer across blood brain barrier in a capillary of the brain. A model of oxygen transport in skeletal muscle using continuously distributed capillaries was proposed by Afas et al [1] where the numerical solution was found to be more efficient than for the discrete capillary problems. In this work, the coupled tissue–capillary PDE system was considered for unidirectional capillary flow in skeletal muscle.

But, in order to fully understand what occurs in microcirculation, it is important to examine how oxygen is transferred and what factors can affect this process. It is also critical to examine the effect of magnetic fields on oxygen transfer since in several situtations, humans must be subjected to such fields. Some examples are during medical testing such as Magnetic Resonance Imaging (MRI) scans and during the treatment of chronic pain or slowly healing ulcers. This highlights the need for such a study which examines the effect that magnetic fields can have on oxygen transfer.

Oxygen is transferred from highly oxygenated blood to surrounding tissue through the blood vessel walls. Thus, in modelling this oxygen transfer, the permeability of these vessel walls cannot be ignored. Certain drugs administered to patients may cause changes to vessel wall permeability [2]. Hence a study which incorporates the wall permeability when examining oxygen transfer is useful in understanding this phenomena in such cases.

2 Methodology

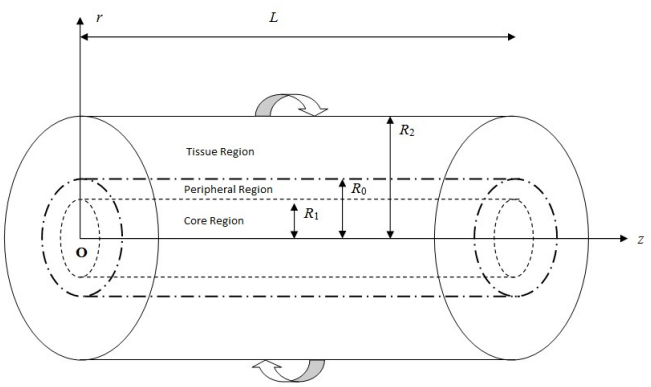

Figure 1. Geometry of the microcirculation in the presence of an external magnetic field.

Consider the flow of blood through microcirculation with permeable walls in the presence of an external magnetic field surrounded by a tissue region. The blood vessel is assumed to be circular, uniform and of semi-infinite extent ($0 \leq z < \infty$) with rigid walls. The two-dimensional cylindrical polar coordinate system is used with z measured along the tube axis and r measured normal to the tube axis. Flow through the blood vessel is assumed to be laminar, axisymmetrical, steady and fully developed. Radius, entrance, end and special wall effects are neglected since the vessel's length is assumed to be much greater than its radius.

A two-layered model is assumed for the blood flow through the vessel of length L, consisting of a central core layer of radius R_1 of erythrocytes suspended in plasma and a peripheral plasma layer of thickness $(R_0 - R_1)$ modelled as a Newtonian fluid. As blood flows through the vessel, oxygen diffuses from the core to the tissue region of radius $(R_2 - R_0)$ passing through the peripheral plasma layer. The geometry of the model used is shown in Figure 1.

2.1 Governing Equations

In the Core Region

In the core region, $0 < r < R_1$, a macroscopic two-phase model is used in the presence of Lorentz's force. The governing equations for the two-phase model are given as follows.

For the fluid (plasma) phase:

$$(1-C)\,\rho_f\left(\frac{\partial u_f}{\partial t}+u_f\frac{\partial u_f}{\partial z}+v_f\frac{\partial u_f}{\partial r}\right)=\begin{array}{c}-(1-C)\,\frac{\partial p_g}{\partial z}+(1-C)\,\mu_s(C)\nabla^2 u_f\\ +CS\,(u_p-u_f)-\sigma B_0^2 u_f,\end{array} \tag{2.1}$$

$$(1-C)\,\rho_f\left(\frac{\partial v_f}{\partial t}+u_f\frac{\partial v_f}{\partial z}+v_f\frac{\partial v_f}{\partial r}\right)=\begin{array}{c}-(1-C)\,\frac{\partial p_g}{\partial r}+CS\,(v_p-v_f)\\ +(1-C)\,\mu_s(C)\left(\nabla^2-\frac{1}{r^2}\right)v_f,\end{array} \tag{2.2}$$

$$\frac{1}{r}\frac{\partial}{\partial r}\left[r\,(1-C)\,v_f\right]+\frac{\partial}{\partial z}\left[(1-C)\,u_f\right]=0. \tag{2.3}$$

For the particle phase:

$$C\rho_p\left(\frac{\partial u_p}{\partial t}+u_p\frac{\partial u_p}{\partial z}+v_p\frac{\partial u_p}{\partial r}\right)=-C\frac{\partial p_g}{\partial z}+CS\,(u_f-u_p)\,, \tag{2.4}$$

$$C\rho_p\left(\frac{\partial v_p}{\partial t}+u_p\frac{\partial v_p}{\partial z}+v_p\frac{\partial v_p}{\partial r}\right)=-C\frac{\partial p_g}{\partial r}+CS\,(v_f-v_p)\,, \tag{2.5}$$

$$\frac{1}{r}\frac{\partial}{\partial r}\left(rCv_p\right)+\frac{\partial}{\partial z}\left(Cu_p\right)=0. \tag{2.6}$$

Here $\nabla^2=\frac{1}{r}\frac{\partial}{\partial r}\left(r\frac{\partial}{\partial r}\right)+\frac{\partial^2}{\partial z^2}$ is a two-dimensional Laplacian operator, (u_f, v_f) and (u_p, v_p) are the (axial, radial) components of the fluid and particle velocities. C denotes the volume fraction density of the particles, p_g is the pressure, $\mu_s(C) \simeq \mu_s$ is the mixture viscosity (apparent or effective viscosity), S is the drag coefficient of interaction for the force exerted by one phase on the other, ρ_f and ρ_p are the actual densities of the material constituting the fluid (plasma) and the particle (erythrocytes) phases respectively, $(1-C)\,\rho_f$ is the fluid phase density and $C\rho_p$ is the particulate phase density, and the subscripts f and p denote the quantities associated with the plasma (fluid) and erythrocyte (particle) phases respectively. The electrical conductivity of the fluid is σ and B_0 is the component of the constant uniform magnetic field which was applied.

The suspension viscosity, μ_s, follows the empirical relation given by

$$\mu_s(C)=\frac{\mu_0}{1-mC}\,,$$

with

$$m=\left(7\times10^{-2}\right)\,exp\left[2.49C+\left(\frac{1107}{T}\right)exp\,(-1.69C)\right],$$

where μ_0 is the fluid viscosity (suspending medium) and T, the temperature of the blood measured on the absolute scale (K) used during measurement [5]. The expression for the drag coefficient of interaction, S, is

$$S = 4.5\left(\frac{\mu_0}{a_0^2}\right)\frac{4+3\left(8C-3C^2\right)^{\frac{1}{2}}+3C}{(2-3C)^2},$$

with a_0 as the particle's radius [19, page 540].

Oxygen transfer in this core region is assumed to be through molecular diffusion and convection with the oxygen and haemoglobin being in chemical equilibrium inside the red blood cells. Hence the steady state mass balance of O_2 in this region is given by

$$D_{rc}\left[\frac{1}{r}\frac{\partial}{\partial r}\left(r\frac{\partial p_1}{\partial r}\right)\right]+D_{zc}\frac{\partial^2 p_1}{\partial z^2}=\left(1+\frac{N}{\alpha_c}\frac{\partial \psi}{\partial p_1}\right)u_f\frac{\partial p_1}{\partial z} \tag{2.7}$$

where p_1 is the partial pressure of the O_2 in the core, $(D_{rc},\, D_{zc})$ are the (radial, axial) components of the diffusion coefficients in the core region, N is the O_2 carrying capacity of the blood, α_c is the solubility coefficient of O_2 in the core and ψ is the fractional saturation of the hemoglobin with O_2.

In the Peripheral Region

In the peripheral region, $R_1 \le r \le R_0$, Navier-Stokes equations in the presence of the Lorentz's force were utilized as follows.

$$\rho_0\left(\frac{\partial u_0}{\partial t}+u_0\frac{\partial u_0}{\partial z}+v_0\frac{\partial u_0}{\partial r}\right)=-\frac{\partial p_g}{\partial z}+\mu_0\nabla^2 u_0-\sigma B_0^2 u_0. \tag{2.8}$$

$$\rho_0\left(\frac{\partial v_0}{\partial t}+u_0\frac{\partial v_0}{\partial z}+v_0\frac{\partial v_0}{\partial r}\right)=-\frac{\partial p_g}{\partial r}+\mu_0\left(\nabla^2-\frac{1}{r^2}\right)v_0. \tag{2.9}$$

$$\frac{1}{r}\frac{\partial}{\partial r}(rv_0)+\frac{\partial u_0}{\partial z}=0, \tag{2.10}$$

where (u_0, v_0) are the (axial, radial) components of the peripheral fluid, μ_0 its viscosity and ρ_0 its density.

In the peripheral plasma layer, oxygen is assumed to be transported by molecular diffusion in both the radial and axial directions and by convection so that a steady mass balance equation for O_2 here is given by

$$D_{rp}\left[\frac{1}{r}\frac{\partial}{\partial r}\left(r\frac{\partial p_0}{\partial r}\right)\right]+D_{zp}\frac{\partial^2 p_0}{\partial z^2}=u_0\frac{\partial p_0}{\partial z}, \tag{2.11}$$

where p_0 is the partial pressure of O_2 in this outer plasma layer, $(D_{rp},\, D_{zp})$ are the (radial, axial) components of the diffusion coefficients.

In the Tissue Region

Oxygen is transported from microcirculation to tissue by diffusion due to the partial pressure gradient differences that exist between the two. Oxygen in the tissue is continuously being used by metabolic consuption in the tissue cells. The presence of interstitial fluid is neglected. Thus in the tissue region $(R_0 < r < R_2)$, the transport of oxygen is assumed to depend on molecular diffusion. This leads to the steady state material balance of oxygen in the tissue to be written as

$$D_{rt}\left[\frac{1}{r}\frac{\partial}{\partial r}\left(r\frac{\partial p_2}{\partial r}\right)\right]+D_{zt}\frac{\partial^2 p_2}{\partial z^2}=\frac{g}{\alpha_t}, \tag{2.12}$$

where p_2 is the partial pressure of the O_2 in the tissue, $(D_{rp},\, D_{zp})$ are the (radial, axial) components of the diffusion coefficients in the tissue region, α_t is the solubility of oxygen in the tissue and g is the rate at which oxygen is consumed. This rate is taken to be a constant according to zero-order chemical kinetics.

2.2 Boundary Conditions

By considering the symmetry that exists along the center line, the continuity of velocities at the interface and the continuity of shear stresses at the interface the following boundary conditions as

$$\frac{\partial u_f}{\partial r} = \frac{\partial u_p}{\partial r} = 0, \quad \text{at } r = 0, \tag{2.13}$$

$$u_0 = u_f\,, \quad \text{at } r = R_1 \tag{2.14}$$

$$\mu_0 \frac{\partial u_0}{\partial r} = (1 - C)\,\mu_s \frac{\partial u_f}{\partial r}, \quad \text{at } r = R_1, \tag{2.15}$$

By considering the slip condition at the boundary, it followed that

$$u_0 = u_B \quad \text{at } r = R_0, \tag{2.16}$$

$$\frac{\partial u_0}{\partial r} = \frac{\alpha_s}{\sqrt{K}}\,(u_B - u_{porous}) \quad \text{at } r = R_0, \tag{2.17}$$

where u_B is the slip velocity, $u_{porous} = -\frac{K}{\mu_0}\frac{dp_g}{dz}$ is the velocity in the permeable boundary, α_s is called the slip parameter and K is the medium's permeability [4, page 197].

The following additional boundary and interface conditions were necessary for this examination of oxygen transfer in microcirculation. Due to the symmetry

$$\text{at } r = 0, \quad \frac{\partial p_1}{\partial r} = 0, \quad 0 \le z \le L. \tag{2.18}$$

Assuming that oxygen diffusion into the tissue occurs only along the vessel-tissue interface and not through the outer wall and annular ends of the tissue

$$\text{at } r = R_2, \quad \frac{\partial p_2}{\partial r} = 0, \quad 0 \le z \le L, \tag{2.19}$$

$$\text{at } z = 0, \quad \frac{\partial p_2}{\partial z} = 0, \quad R_0 < r < R_2, \tag{2.20}$$

$$\text{at } z = L, \quad \frac{\partial p_2}{\partial z} = 0, \quad R_0 < r < R_2. \tag{2.21}$$

The partial pressure of the oxygen on entry into the capillary is assumed to be equal to that of the arterial blood

$$\text{at } z = 0, \quad p_1 = p_a, \quad 0 < r < R_1, \tag{2.22}$$

$$\text{at } z = 0, \quad p_0 = p_a, \quad R_1 < r < R_0, \tag{2.23}$$

where p_a is the partial pressure of O_2 in the arterial blood.

At the exit of the capillary, no diffusive flux conditions are assumed

$$\text{at } z = L, \quad \frac{\partial p_1}{\partial z} = 0, \quad 0 < r < R_1, \tag{2.24}$$

$$\text{at } z = L, \quad \frac{\partial p_0}{\partial z} = 0, \quad R_1 < r < R_0. \tag{2.25}$$

Across the interface in the blood between its two layers, the partial pressure of oxygen and its flux are both assumed to be continuous

$$\text{at } r = R_1, \quad p_0 = p_1, \quad 0 \le z \le L, \tag{2.26}$$

$$\text{at } r = R_1, \quad \alpha_c D_{rc} \frac{\partial p_1}{\partial r} = \alpha_p D_{rp} \frac{\partial p_0}{\partial r}, \quad 0 \le z \le L. \tag{2.27}$$

Additionally, across the interface between the blood and the tissue, the partial pressure of oxygen and its flux are both assumed to be continuous

$$\text{at } r = R_0, \quad p_0 = p_2, \quad 0 \le z \le L, \tag{2.28}$$

$$\text{at } r = R_0, \quad \alpha_p D_{rp} \frac{\partial p_0}{\partial r} = \alpha_t D_{rt} \frac{\partial p_2}{\partial r}, \quad 0 \le z \le L, \tag{2.29}$$

where α_p is the solubility coefficient of oxygen in the plasma region.

2.3 Non-dimensional Analysis

In order to use the assumptions taken to simplify the equations involved in this problem, a non-dimensional analysis must first be conducted using the following,

$$r^* = \frac{r}{R_0},\ z^* = \frac{z}{R_0},\ a_0^* = \frac{a_0}{R_0},\ \mu_s^* = \frac{\mu_s}{\mu_0},\ t^* = \frac{tU_0}{R_0},\ p_g^* = \frac{p_g R_0}{U_0 \mu_0},\ S^* = \frac{SR_0^2}{\mu_0},$$

$$(u_0^*, u_f^*, u_p^*) = \frac{(u_0, u_f, u_p)}{U_0},\ (v_0^*, v_f^*, v_p^*) = \frac{(v_0, v_f, v_p)}{U_0},\ (p_0^*, p_1^*, p_2^*) = \frac{(p_0, p_1, p_2)}{p_c},$$

$$M^2 = \frac{\sigma B_0^2 R_0^2}{\mu_0},\ Re_f = \frac{\rho_f R_0 U_0}{\mu_0},\ Re_p = \frac{\rho_p R_0 U_0}{\mu_0},\ Re_0 = \frac{\rho_0 R_0 U_0}{\mu_0},\ Pe = \frac{R_0 U_0}{D_{rp}}$$

where U_0 and p_c are the characteristic velocity and partial pressure respectively, M is the Hartmann number, (Re_f, Re_p, Re_0) is Reynold's number of the (fluid phase, particle phase,outer fluid) and Pe is the Peclet number.

Assuming further that $v_f = v_p = v_0 = 0$, $Re_f \ll 1$, $Re_p \ll 1$, $Re_0 \ll 1$ and neglecting $\frac{\partial^2 u_f}{\partial z^2}, \frac{\partial^2 u_p}{\partial z^2}$ and $\frac{\partial^2 u_0}{\partial z^2}$, the non-dimensional system of equations given by,

$$(1-C)\frac{dp_g}{dz} = (1-C)\frac{\mu_s}{r}\frac{\partial}{\partial r}\left(r\frac{\partial u_f}{\partial r}\right) + CS\left(u_p - u_f\right) - M^2 u_f,$$

$$C\frac{dp_g}{dz} = CS\left(u_f - u_p\right),$$

$$\frac{dp_g}{dz} = \frac{1}{r}\frac{\partial}{\partial r}\left(r\frac{\partial u_0}{\partial r}\right) - M^2 u_0,$$

will be solved subject to,

$$\frac{\partial u_f}{\partial r} = \frac{\partial u_p}{\partial r} = 0, \quad \text{at } r = 0, \tag{2.30}$$

$$u_0 = u_f\,, \quad \text{at } r = \gamma_1 \tag{2.31}$$

$$\frac{\partial u_0}{\partial r} = (1-C)\mu_s \frac{\partial u_f}{\partial r}\,, \quad \text{at } r = \gamma_1, \tag{2.32}$$

$$u_0 = u_B, \quad \text{at } r = 1, \tag{2.33}$$

$$\frac{\partial u_0}{\partial r} = \frac{\alpha_s}{\sqrt{D_a}}\left(u_B + D_a \frac{dp_g}{dz}\right), \quad \text{at } r = 1. \tag{2.34}$$

Additionally, the non-dimensional system of equations given as,

$$\frac{\partial^2 p_0}{\partial r^2} + \frac{1}{r}\frac{\partial p_0}{\partial r} + \frac{D_{zp}}{D_{rp}}\frac{\partial^2 p_0}{\partial z^2} = Pe\, u_0 \frac{\partial p_0}{\partial z}, \tag{2.35}$$

$$\frac{D_{rc}}{D_{rp}}\left(\frac{\partial^2 p_1}{\partial r^2} + \frac{1}{r}\frac{\partial p_1}{\partial r}\right) + \frac{D_{zc}}{D_{rp}}\frac{\partial^2 p_1}{\partial z^2} = Pe\ (1 + \phi(p_1))\, u_f \frac{\partial p_1}{\partial z}, \tag{2.36}$$

$$\frac{\partial^2 p_2}{\partial r^2} + \frac{1}{r}\frac{\partial p_2}{\partial r} + \frac{D_{zt}}{D_{rp}}\frac{\partial^2 p_2}{\partial z^2} = G, \tag{2.37}$$

was solved subject to its boundary conditions. The function $\phi(p_1)$ is proportional to the slope of the oxygen dissociation curve which is given by

$$\phi(p_1) = \frac{N}{\alpha_c p_c}\frac{\partial \psi}{\partial p_1}.$$

The function $\psi(p_1)$ is yielded from the assumption that the chemical reaction between oxygen and haemoglobin is in equlibrium. In equilibrium, the chemical reactions occur instantaneously and the partial pressure of oxygen in hematocrit and plasma are equal. Many forms of the equation can be used to represent the oxygen dissociation curve (ODC). In this analysis, Hill's equation was used as

$$\psi(p_1) = \frac{\left(\frac{p_1}{p_{50}}\right)^n}{1 + \left(\frac{p_1}{p_{50}}\right)^n},$$

where p_1 is dimensional partial pressure, p_{50} is the partial pressure of O_2 at the 50 % saturation of hemoglobin with O_2 and n is the Hill parameter [20, page 560].

Utilizing Hill's equation, it followed that

$$\frac{\partial \psi}{\partial p_1} = \frac{n\, p_{50}^n p_c^n p_1^{n-1}}{\left(p_{50}^n + p_1^n p_c^n\right)^2},$$

and

$$\phi(p_1) = \frac{N\, n\, p_{50}^n \left(p_c p_1\right)^{n-1}}{\alpha_c \left[p_{50}^n + \left(p_c p_1\right)^n\right]^2}.$$

The relevant boundary conditions resulted.

$$\frac{\partial p_1}{\partial r} = 0, \quad 0 \le z \le \frac{L}{R_0}. \tag{2.38}$$

$$\text{at } r = R, \quad \frac{\partial p_2}{\partial r} = 0, \quad 0 \le z \le \frac{L}{R_0}, \tag{2.39}$$

$$\text{at } z = 0, \quad \frac{\partial p_2}{\partial z} = 0, \quad 1 < r < R, \tag{2.40}$$

$$\text{at } z = \frac{L}{R_0}, \quad \frac{\partial p_2}{\partial z} = 0, \quad 1 < r < R. \tag{2.41}$$

$$\text{at } z = 0, \quad p_1 = p_a, \quad 0 < r < \gamma_1, \tag{2.42}$$

$$\text{at } z = 0, \quad p_0 = p_a, \quad \gamma_1 < r < 1. \tag{2.43}$$

$$\text{at } z = \frac{L}{R_0}, \quad \frac{\partial p_1}{\partial z} = 0, \quad 0 < r < \gamma_1, \tag{2.44}$$

$$\text{at } z = \frac{L}{R_0}, \quad \frac{\partial p_0}{\partial z} = 0, \quad \gamma_1 < r < 1. \tag{2.45}$$

$$\text{at } r = \gamma_1, \quad p_0 = p_1, \quad 0 \le z \le \frac{L}{R_0}, \tag{2.46}$$

$$\text{at } r = \gamma_1, \quad \frac{\partial p_0}{\partial r} = \frac{\alpha_c D_{rc}}{\alpha_p D_{rp}}\frac{\partial p_1}{\partial r}, \quad 0 \le z \le \frac{L}{R_0}. \tag{2.47}$$

$$\text{at } r = 1, \quad p_0 = p_2, \quad 0 \le z \le \frac{L}{R_0}, \tag{2.48}$$

$$\text{at } r = 1, \quad \frac{\partial p_0}{\partial r} = \frac{\alpha_t D_{rt}}{\alpha_p D_{rp}}\frac{\partial p_2}{\partial r}, \quad 0 \le z \le \frac{L}{R_0}. \tag{2.49}$$

3 Results

The solution for the velocities, u_0 and u_f were found to be

$$u_0 = k_1 I_0(Mr) + k_2 K_0(Mr) - \frac{1}{M^2}\left(\frac{dp}{dz}\right), \ \gamma_1 \le r \le 1, \tag{3.1}$$

$$u_f = k_3 J_0(M\gamma r) - \frac{1}{M^2}\left(\frac{dp}{dz}\right), \ 0 \le r \le \gamma_1, \tag{3.2}$$

where

$$k_1 = \frac{\frac{1}{M^2}\frac{dp}{dz} - k_2 K_0(M) + u_B}{I_0(M)}, \tag{3.3}$$

$$k_2 = \left(\frac{dp}{dz}\right)\frac{\xi_1\left(\xi_4 + \frac{1}{M^2}\xi_5\right)}{\xi_2\,\xi_5 - \xi_1\,\xi_3}, \tag{3.4}$$

$$k_3 = \frac{k_2 K_1(M\gamma_1) - k_1 I_1(M\gamma_1)}{(1-C)\mu_s \gamma J_1(M\gamma\gamma_1)}, \tag{3.5}$$

$$u_B = \frac{k_2\,\xi_3 + \xi_4\,\frac{dp}{dz}}{\xi_5}, \tag{3.6}$$

where

$$\xi_1 = (1-C)\mu_s\gamma I_0(M\gamma_1)J_1(M\gamma\gamma_1) + I_1(M\gamma_1)J_0(M\gamma\gamma_1),$$

$$\begin{aligned}\xi_2 = {} & I_0(M)\left[J_0(M\gamma\gamma_1)K_1(M\gamma_1) - (1-C)\mu_s\gamma J_1(M\gamma\gamma_1)K_0(M\gamma_1)\right] \\ & + \xi_1 K_0(M),\end{aligned}$$

$$\xi_3 = M\sqrt{D_a}\left[I_0(M)K_1(M) + I_1(M)K_0(M)\right],$$

$$\xi_4 = \frac{\sqrt{D_a}}{M}\left[M\alpha_s\sqrt{D_a}I_0(M) - I_1(M)\right],$$

$$\xi_5 = M\sqrt{D_a}\,I_1(M) - \alpha_s\,I_0(M),$$

and

$$\gamma = \sqrt{\frac{1}{(C-1)\mu_s}},$$

where J_n is the bessel function of first kind of order n, I_n is the modified bessel function of the first kind of order n, K_n is the modified bessel function of the second kind of order n and k_1, k_2, k_3 and γ are constants.

Assuming that the axial diffusion in the tissue region is small compared to radial diffusion $\left(\frac{\partial^2 p_2}{\partial z^2} = 0\right)$ it follows that

$$\frac{\partial}{\partial r}\left(r\frac{\partial p_2}{\partial r}\right) = rG. \tag{3.7}$$

Using integration and the boundary conditions from equations 2.39 and 2.48 resulted in

$$p_2(r,z) = p_0(1,z) + \frac{G}{2}\left(\frac{r^2-1}{2} - R^2 ln(r)\right). \tag{3.8}$$

The Galerkin finite element method was used to obtain the solution for mass transfer in the blood vessel region. Firstly, the domain was discretized into a set of finite elements. The blood vessel region enclosed by surface, S, was divided into a finite number of elements. In this analysis, the blood vessel region was split into two, the core and peripheral regions. A mesh was generated over each region. Isoparametric, curvilinear, quadrilateral elements were chosen since this is a suitable type of element for these regions under consideration. Each element contained eight

nodes. Thus the eight node quadratic rectangular (serendipity) element was used. A mesh was generated to represent these regions and a finite element solution was found over the mesh (see Figure 2). The mesh was refined accordingly to obtain an approximate solution within a suitable error tolerance, ϵ. The analytic solution was then utilized to find the solution in the third region, the tissue region.

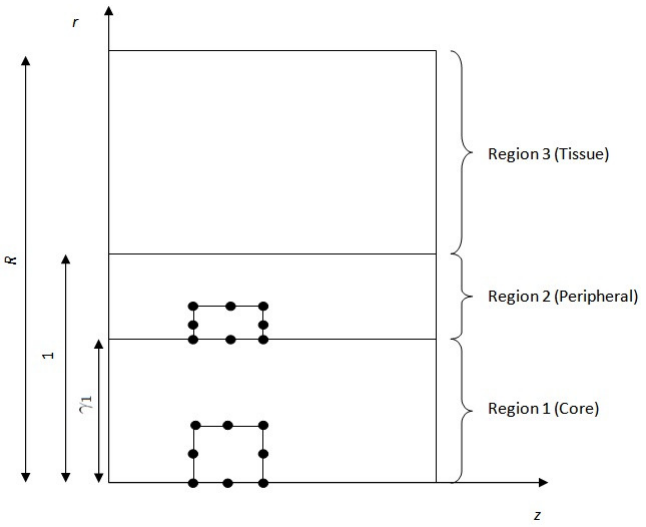

Figure 2. The three different regions of the problem and a typical element in the core and peripheral region.

The weak (or weighted integral) formulation of the governing differential equations was obtained as follows. Both equations 2.35 and 2.36 are of the form,

$$A\left(\frac{\partial^2 p}{\partial r^2}+\frac{1}{r}\frac{\partial p}{\partial r}\right)+B\frac{\partial^2 p}{\partial z^2}=PeV(p)\frac{\partial p}{\partial z}. \tag{3.9}$$

For the plasma region in equation 3.9, $A=1$, $B=\frac{D_{zp}}{D_{rp}}$ and $V(p)=u_0$ and for the core region, $A=\frac{D_{rc}}{D_{rp}}$, $B=\frac{D_{zc}}{D_{rp}}$ and $V(p)=(1+\phi(p))\,u_f$.

In the development of the weak form, a typical element need only be considered. Assuming Ω_e is a typical (quadrilateral) element of the finite element mesh, the following Galerkin's finite element model over Ω_e was used.

Multiplying equation 3.9 by a weight function, w, which is assumed to be differentiable with respect to r and z, and then integrating over the element domain gave

$$\int_{\Omega_e} w\left[-A\left(\frac{\partial^2 p}{\partial r^2}+\frac{1}{r}\frac{\partial p}{\partial r}\right)-B\frac{\partial^2 p}{\partial z^2}+PeV(p)\frac{\partial p}{\partial z}\right]d\Omega^e=0,$$

$$2\pi\int_z\int_r w\left\{-A\left[\frac{1}{r}\frac{\partial}{\partial r}\left(r\frac{\partial p}{\partial r}\right)\right]-B\frac{\partial}{\partial z}\left(\frac{\partial p}{\partial z}\right)+PeV(p)\frac{\partial p}{\partial z}\right\}r\,drdz=0.$$

Integrating the highest order term by parts resulted in

$$\begin{array}{c}2\pi\int_z\int_r\left(A\frac{\partial w}{\partial r}\frac{\partial p}{\partial r}+B\frac{\partial w}{\partial z}\frac{\partial p}{\partial z}+wPeV(p)\frac{\partial p}{\partial z}\right)r\,drdz\\ -2\pi\oint_{\Gamma_e} w\left(rA\frac{\partial p}{\partial r}n_r+rB\frac{\partial p}{\partial z}n_z\right)dS^e\end{array}=0,$$

$$\int_z\int_r\left(A\frac{\partial w}{\partial r}\frac{\partial p}{\partial r}+B\frac{\partial w}{\partial z}\frac{\partial p}{\partial z}+wPeV(p)\frac{\partial p}{\partial z}\right)r\,drdz-\oint_{\Gamma_e} wq_n\,dS^e=0,$$

where $q_n=r\left(A\frac{\partial p}{\partial r}n_r+B\frac{\partial p}{\partial z}n_z\right)$ is the normal flux with n_r and n_z are the axial and radial component of the outward unit normal vector to the surface element dS^e on the boundary Γ_e.

By Galerkin's Finite Element Method, it was assumed $p(r,z)$ was approximated by the finite element interpolation p_h^e over the element Ω_e such that

$$p \approx p_h^e(z,r) = \sum_{j=1}^{n} p_j^e \psi_j^e(z,r)$$

where $\psi_j^e(z,r)$ are the interpolation functions and that $w = \psi_i^e$.

Substituting these gave

$$\sum_{j=1}^{n} \left[\int_z \int_r \left(\begin{array}{c} A\frac{\partial \psi_i^e}{\partial r}\frac{\partial \psi_j^e}{\partial r} + B\frac{\partial \psi_i^e}{\partial z}\frac{\partial \psi_j^e}{\partial z} \\ +\psi_i^e PeV(p)\frac{\partial \psi_j^e}{\partial z} \end{array} \right) p_j^e \; r dr dz \right] - \oint_{\Gamma_e} \psi_i^e q_n \, dS^e = 0,$$

$$\sum_{j=1}^{n} K_{ij}^e p_j^e - Q_i^e = 0,$$

$$\sum_{j=1}^{n} K_{ij}^e p_j^e = Q_i^e,$$

$$\left[K_{ij}^e\right] \{p^e\} = \{Q_i^e\},$$

with $[K_{ij}^e] = [K_{1ij}^e] + [K_{2ij}^e]$ where

$$K_{1ij}^e = \int_z \int_r \left(A\frac{\partial \psi_i^e}{\partial r}\frac{\partial \psi_j^e}{\partial r} + B\frac{\partial \psi_i^e}{\partial z}\frac{\partial \psi_j^e}{\partial z} \right) r \, dr dz, \tag{3.10}$$

$$K_{2ij}^e = \int_z \int_r \left(\psi_i^e \, Pe \, V(p) \frac{\partial \psi_j^e}{\partial z} \right) r \, dr dz, \tag{3.11}$$

and

$$Q_i^e = \oint_{\Gamma_e} \psi_i^e q_n \, dS^e, \tag{3.12}$$

with $i, \, j = 1, \, 2, \, \ldots n$.

Hence there is a need for n independent algebraic equations to be able to solve for the n unknowns, $p_1^e, \, p_2^e, \ldots p_n^e$. This led to n linearly independent functions $\psi_1^e, \psi_2^e, \ldots, \psi_n^e$ being chosen. Before this matrix system was solved, the boundary conditions involved were enforced. The matrix system obtained was then solved to obtain the values of p,

$$\{p^e\} \quad = \quad \left[K_{ij}^e\right]^{-1} \{Q_i^e\}.$$

Note that this problem is nonlinear so a fixed point iterative technique was necessary to solve for the p values. The iterative technique continued until

$$\sum_{i=1}^{m_t} \left| \left[p_i^{r+1} - p_i^r \right] \right| < \epsilon,$$

where r represents the r^{th} iteration, m_t is the total number of nodes in the solution domain and ϵ is the error of tolerance.

The following are the values of the parameters used in the computations [14], [15].

Parameter	Value	units
D_{rb}	1.12×10^{-5}	$cm^2 sec^{-1}$
D_{zb}	1.95×10^{-4}	$cm^2 sec^{-1}$
D_{rt}	1.7×10^{-5}	$cm^2 sec^{-1}$
N_b	9.1×10^{-6}	$mol\, cm^{-3}$
n	2.6472	
p_c	100	$mmHg$
p_{50}	27.2	$mmHg$
α_c	1.527×10^{-9}	$mol\, cm^{-3}(mmHg)^{-1}$
α_p	1.527×10^{-9}	$mol\, cm^{-3}(mmHg)^{-1}$
α_t	1.295×10^{-9}	$mol\, cm^{-3}(mmHg)^{-1}$
g	3.72×10^{-8}	$mol\, cm^{-3} s^{-1}$
R_0	3.25×10^{-4}	cm
R_2	3.25×10^{-3}	cm
ϵ	10^{-7}	

Table 1. Parameter values utilized in this study.

Plots for the solutions were provided using the following parameter values $\frac{dp_g}{dz} = -70, -90, -110$; $p_a = 75, 95, 115\, mmHg$; $C = 0.2, 0.4, 0.6$; $\gamma_1 = 0.5, 0.6, 0.7$; $Pe = 0.435, 0.87, 1.74$; $M = 2, 4, 6$; $\sqrt{D_a} = 0.02, 0.03, 0.04$ with $\alpha_s = 0.3$. The radius of the red cell was assumed to be $4\,\mu m$ and the experimental temperature used to find m was $25.5\,^oC$ [8]. The length of the vessel was assumed to be sixty times its radius [15, page 115]. All plots included the presence of the magnetic field and permeable walls.

Assuming, $H_b = H_c = C$ and given the experimental values for D_{rb} and D_{zb}, values for D_{rp}, D_{zp}, D_{rc} and D_{zc} were computed. These were computed using [6]

$$\frac{D_p}{D_b} = \frac{1.58 + 0.64\, H_b}{1.58 - 0.78\, H_b}. \tag{3.13}$$

where D_p and D_b are the diffusion coefficients in the plasma and blood respectively. After computing the values for D_{rp} and D_{zp} using equation 3.13, the corresponding values for diffusion in the core region, D_{rc} and D_{zc}, were computed [17, page 424].

Graphs were generated to observe the effect of varying different parameters on the partial pressure of oxygen. Since partial pressure is directly proportional to concentration, variations with respect to the partial pressure can be used to investigate the oxygen concentration in the vessel and the tissue region. Non-zero positive values for M and $\sqrt{D_a}$ indicate the presence of an external magnetic field and permeable vessel walls.

In figure 3, a single mesh plot was generated to observe the partial pressure in all three regions utilizing the numerical solution in the vessel and the analytical solution in the tissue region. The shape of this curve highly correlates with the work of Whiteley, Gavaghan and Hahn [22, page 517].

In figure 3, it is clear that there was a decline in the partial pressure of oxygen in both the radial and axial directions. As oxygenated blood entered the vessel and flowed in the axial direction, the concentration of oxygen decreased because it was constantly being diffused from its region of high concentration in the vessel to its region of low concentration in the tissue. The difference in the partial pressures in each region drove this diffusion.

In the radial direction, the concentation of oxygen was at its maximum at the core of the vessel and there was a very small decrease of oxygen from the core region to the plasma region. Radially along the tissue region, there was a decline in the concentration of oxygen. This was also observed in the analysis of [18, page 27]. Traversing further away from the vessel, less oxygen was available for diffusion since it was constantly being consumed by the tissue cells encountered.

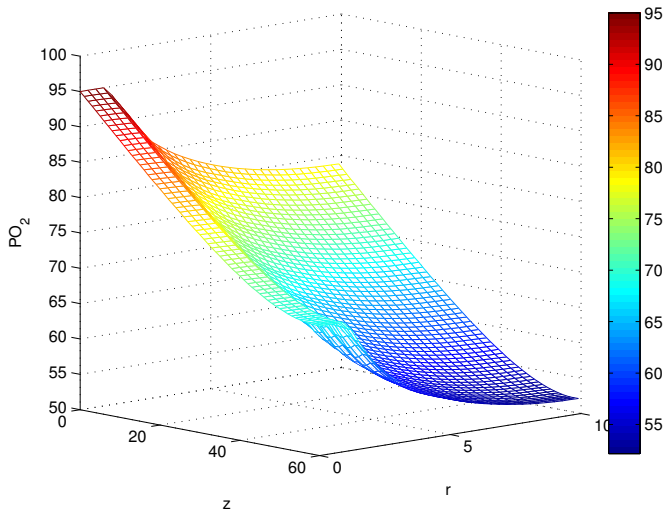

Figure 3. Mesh plot of partial pressures (with $\frac{dp_g}{dz} = -70$, $p_a = 95$, $C = 0.4$, $\gamma_1 = 0.8$, $Pe = 0.435$, $M = 4$ and $\sqrt{D_a} = 0.02$).

This decrease in the oxygen concentration in both directions resulted in the partial pressure of oxygen achieving its minimum value at the end point of the tissue region when $r = 10$ and at the end of the vessel when $z = 60$.

Inside the vessel, the amount of red blood cells present and the thickness of the plasma layer are two important factors that can affect the concentration and delivery of oxygen respectively. As the hematocrit value, C, increased, the partial pressure values were higher in all three regions as shown in figure 4. Since hematocrit is the ratio of the volume of red blood cells to the total volume of blood, there is a greater concentration of oxygen present in both the vessel and tissue as the number of red blood cells increase.

Thus under conditions where the red blood cell count in the blood is lower than normal, for example in patients with plasma cell dyscrasias or Hb SS-sickle cell, there is less O_2 present in the blood and tissue. This can be detrimental to the surrounding tissue as it becomes starved of oxygen. Meanwhile, in patients with high hematocrit, for example those with polycythemia, there is a high oxygen concentration in the tissue. If the oxygen level in the body becomes too high, oxygen toxicity develops which leads to a condition known as hyperoxemia. This can result in twitching, dizziness, nausea, seizures and in severe cases can even be fatal.

It was also observed that the thickness of the plasma layer affected the delivery of oxygen to the tissue. Figure 5 presented the effect of increasing the core region thickness on PO_2. It must be noted that changes to the core region thickness from $\gamma_1 = 0.5$ to 0.6 up to 0.7 corresponded to the plasma layer thickness decreasing from 0.5 to 0.4 down to 0.3. Thus, as the plasma layer became thinner, the partial pressure in the vessel and tissue increased. This showcases that the plasma layer acts as a barrier which reduces the transfer of oxygen from the core to the tissue region which is in keeping with the work of [17, page 425]. Thus as this layer thins, the oxygen content elevates.

The intensity of the magnetic field also influenced the concentration of oxygen present in the vessel and tissue. From figure 6, PO_2 decreased with increases in the Hartmann number. Since the Hartmann number is a reflection of the strength of the magnetic field, as the magnetic field intensified, there was a drop in the concentration of oxygen present in all three regions. Thus for patients exposed to a magnetic field of increasing magnitude, a diminishing supply of oxygen will be present in their vessels and also a lower concentration of oxygen will be present in their tissues which can lead to life threatening hypoxemia or hypoxia.

Increasing the magnetic field intensity resulted in a greater decline in the oxygen content in the vessel and the tissue. This is in keeping with previous work and compounds the argument that such high intensity magnetic fields should be avoided [3, page 1704].

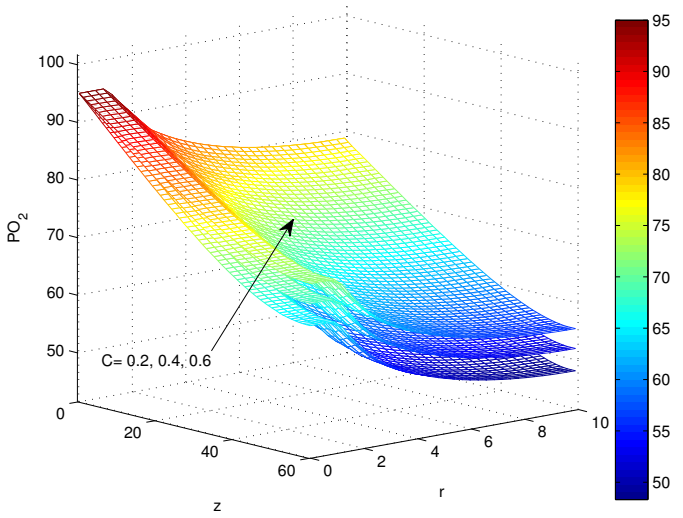

Figure 4. Mesh plot of partial pressures for varying hematocrit (with $\frac{dp_g}{dz} = -70$, $p_a = 95$, $\gamma_1 = 0.8$, $Pe = 0.435$, $M = 4$ and $\sqrt{D_a} = 0.02$).

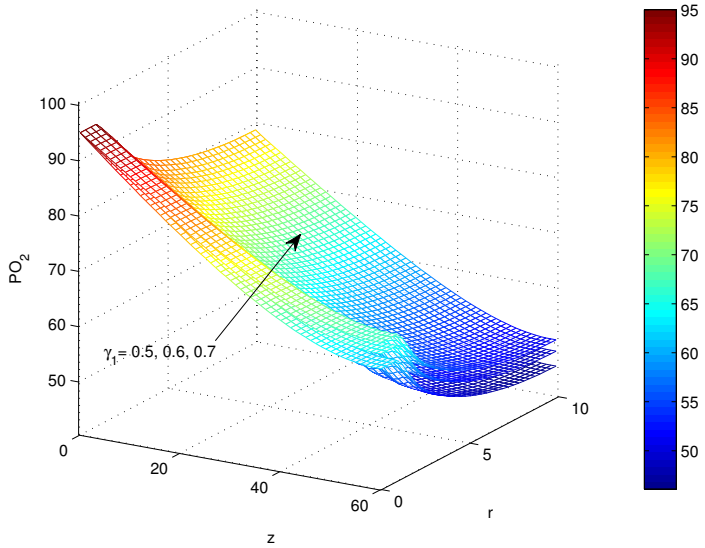

Figure 5. Mesh plot of partial pressures for varying core region thickness (with $\frac{dp_g}{dz} = -70$, $C = 0.4$, $p_a = 95$, $Pe = 0.435$, $M = 4$ and $\sqrt{D_a} = 0.02$).

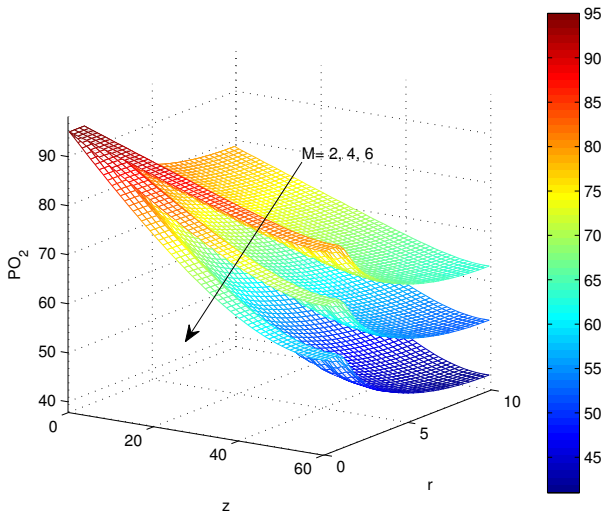

Figure 6. Mesh plot of partial pressures for varying Hartmann numbers (with $\frac{dp_g}{dz} = -70$, $C = 0.4$, $p_a = 95$, $\gamma_1 = 0.8$, $P_c = 0.435$ and $\sqrt{D_a} = 0.02$).

Figure 7 highlighted the effect that wall permeability had on oxygen concentration. Changes to the Darcy number are proportional to changes in the vessel wall's permeability. Figure 7 indicated that there was a decrease in the concentration of oxygen in all three regions as the vesssel walls became more permeable. A decline in the PO_2 in the axial direction was observed as Darcy number was increased.

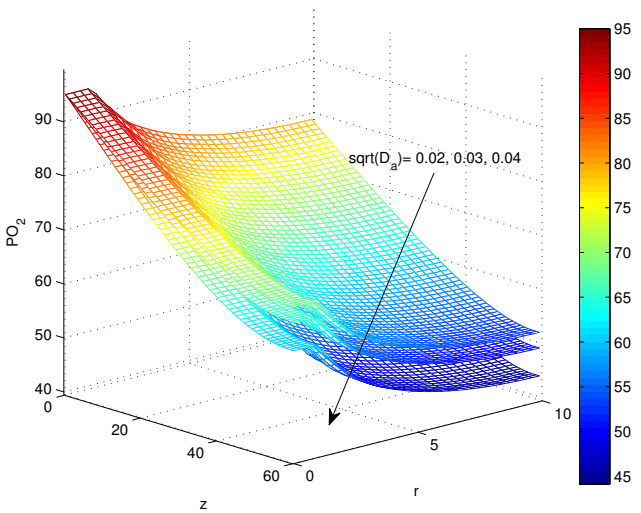

Figure 7. Mesh plot of partial pressures for varying Darcy numbers (with $\frac{dp_g}{dz} = -70$, $C = 0.4$, $p_a = 95$, $\gamma_1 = 0.8$, $P_c = 0.435$ and $M = 4$).

Therefore, patients who take medications which affect wall permeability (such as ACE inhibitors, calcium-channel blockers, decongestants, beta blockers, antihistamines and sildenafil nonsteroidal and anti-inflammatory can expect a change in the concentration of oxygen present in their tissues. Both cases of low or high oxygen levels are harmful, thus the effect that these drugs has on oxygen transfer must be monitored closely especially in cases where they must be used by a patient for a long period of time.

3.1 Conclusion

The transfer of oxygen from microcirculation to tissue was examined. Blood flow in the vessel was modelled using a suitable two-layered flow with a core region as a suspension of red blood cells in fluid and a peripheral plasma layer. The walls were considered to be permeable and an external magnetic field was present. A finite element method was used to solve the system of differential equations which arose in the core region and the solution in the tissue region was solved analytically.

Based on the computations and graphical outputs obtained, the following were observed.

- The partial pressure of oxygen decreased in the axial and radial directions. The difference in the PO_2 values from the core to the plasma to the tissue region drove the O_2 diffusion.
- There was an increase in the partial pressure of O_2 in all three regions with increases to the magnitude of the hematocrit and core region thickness.
- The partial pressure of O_2 decreased with increasing magnetic field strength and wall permeability.

Future work based on this study should include the presence of stenosis in order to examine oxygen transfer from microcirculation to tissue in cardiovascular patients.

References

[1] K. C. Afas, R. Vijay and D. Goldman, A two-compartment model of oxygen transport in skeletal muscle using continuously distributed capillaries, *Math. Biosci.* **333** (2021).

[2] S. American, Common prescription drugs alter blood's flow, https://www.scientificamerican.com/article/common-prescription-drugs-alter-blood-s-flow/ (2014).

[3] R. Bali and U. Awasthi, Study of an oxygenation process in capillary in the presence of magnetic field, *Int. J. Math. Anal.* **35**, 1679–1706 (2010).

[4] G. S. Beavers and D. D. Joseph, Boundary conditions at a naturally permeable wall, *J. Fluid Mech.* **30** (1), 197–207 (1967).

[5] S. E. Charm and G. S. Kurland, *Blood Flow and Microcirculation*, Wiley, New York (1974).

[6] W. J. Dorson and M. E. Voorhees, *Artificial Lungs for Acute Respiratory Failure*, Academic Press, New York (1976).

[7] A. O. Frank, C. Chuong and R. L. Johnson, A Finte-Element Model of oxygen diffusion in the pulmonary capillaries, *J. Appl. Physiol.* **82**, 2036–2044 (1997).

[8] A. C. Guyton and J. E. Hall, *Textbook of Medical Physiology*, Elsevier Saunders, Pennsylvania (2006).

[9] M. Hassanzadeganroudsari, M. Soltani, A. Heydarinasab, A. T. Nakhjiri, M. D. K. Hossain and A. A. Khiyavi, Mathematical modeling and simulation of molecular mass transfer across blood brain barrier in brain capillary, *J. Mol. Liq.* **310** (2020).

[10] A. Kaesler, M. Rosen, T. Schmitz-Rode, U. Steinseifer and J. Arens, Computational modeling of oxygen transfer in artificial lungs, *Artif. Organs* **42** (8), 786–799 (2018).

[11] A. Krogh, The Supply of oxygen to the tissue and the regulation of the capillary circulation, *J. Physiol.* **52**, 457–474 (1919).

[12] P. Kumar, *Finite Element Analysis of mass transfer in creeping fluid flow through tubes: Application to blood flow*, PhD diss., Indian Institute of Technology (1982).

[13] A. Lucker, B. Weber and P. Jenny, A Dynamic model of oxygen transport from capillaries to tissue with moving red blood cells, *Am. J. Physiol. - Heart Circ. Physiol.* **308** (3), 206–216 (2015).

[14] D. D. Reneau, D. F. Bruley and M. H. Knisely, *Chem. Eng. Med. Sci. Biol.*, Plenum Press, New York (1967).

[15] M. Sharan, B. Singh, M. P. Singh and P. Kumar, Finite Element Analysis of oxygen transport in the systemic capillaries, *IMS: J. Math. Appl. Med. Biol.* **8**,107–123 (1991).

[16] M. Sharan, M. P. Singh and B. Singh, A mathematical model for the simultaneous transport of O_2 and CO_2 in the systemic capillaries and surrounding tissue in a hyperbaric environment with first order metabolism, *Nonlinear World* **1**, 255–276 (1995).

[17] M. Sharan, B. Singh and P. Kumar, A two-layer model for studying the effect of plasma layer on the delivery of oxygen to tissue using a finite element method, *Appl. Math. Model.* **21**, 419–426 (1997).

[18] M. Sharan, M. P. Singh, and I. Sud, Modelling of O_2 transport in the systemic circulation in a hyperbaric environment, *Front. Med. Biol. Eng.* **3**, 27–44 (1991).

[19] C. K. W. Tam, The drag on a cloud of spherical particles in low reynolds number flow, *J. Fluid Mech.* **38**, 537–546 (1969).

[20] J. Ulatowski, T. Nishikawa, B. Matheson-Urbaitis, E. Bucci, R. Traystman and R. Koehler, Regional blood flow alterations after bovine fumaryl beta beta-crosslinked hemoglobin transfusion and nitric oxide synthase inhibition, *Crit. Care Med.* **24** (4), 558–565 (1996).

[21] A. Vadapalli, D. Goldman and A. Popel, Calculations of oxygen transport by red blood cells and hemoglobin solutions in capillaries, *Artif. Cells Blood Substit. Immobil. Biotechnol.* **30** (3), 157–188 (2002).

[22] J. P. Whiteley, D. J. Gavaghan and C. E. W. Hahn, Mathematical modelling of oxygen transport to tissue, *J. Math. Biol.* **44** (6), 503–522 (2002).

[23] M. Zahorodny-Burke, M. B. Nearingburg, and A. L. Elias, Finite Element Analysis of oxygen transport in microfluidic cell culture devices with varying channel architecures, perfusion rates and materials, *Chem. Eng. Sci.* **66**, 6244–6253 (2011).

Author information

Alana R. Sankar, Sreedhara Rao Gunakala and Donna M. G. Comissiong, Department of Mathematics and Statistics, The University of the West Indies, St. Augustine, Trinidad & Tobago.
E-mail: Alana.Sankar@sta.uwi.edu, Sreedhara.Rao@sta.uwi.edu, Donna.Dyer@sta.uwi.edu